Water Mass Transformation in the Greenland Sea during the Period 1986–2016

AILIN BRAKSTAD, KJETIL VÅGE, AND LISBETH HÅVIK

Geophysical Institute, University of Bergen, and Bjerknes Centre for Climate Research, Bergen, Norway

G. W. K. MOORE

Department of Physics, University of Toronto, Toronto, Ontario, Canada

ABSTRACT

Hydrographic measurements from ships, autonomous profiling floats, and instrumented seals over the period 1986–2016 are used to examine the temporal variability in open-ocean convection in the Greenland Sea during winter. This process replenishes the deep ocean with oxygen and is central to maintaining its thermohaline properties. The deepest and densest mixed layers in the Greenland Sea were located within its cyclonic gyre and exhibited large interannual variability. Beginning in winter 1994, a transition to deeper (>500 m) mixed layers took place. This resulted in the formation of a new, less dense class of intermediate water that has since become the main product of convection in the Greenland Sea. In the preceding winters, convection was limited to <300-m depth, despite strong atmospheric forcing. Sensitivity studies, performed with a one-dimensional mixed layer model, suggest that the deeper convection was primarily the result of reduced water-column stability. While anomalously fresh conditions that increased the stability of the upper part of the water column had previously inhibited convection, the transition to deeper mixed layers was associated with increased near-surface salinities. Our analysis further suggests that the volume of the new class of intermediate water has expanded in line with generally increased depths of convection over the past 10–15 years. The mean export of this water mass from the Greenland Sea gyre from 1994 to present was estimated to be 0.9 ± 0.7 Sv (1 Sv $\equiv 10^6$ m^3 s^{-1}), although rates in excess of 1.5 Sv occurred in summers following winters with deep convection.

1. Introduction

The Nordic seas (Fig. 1) are a key region for dense water formation that impacts climate on a global scale (e.g., Gebbie and Huybers 2010). Warm Atlantic water (AW) flows northward into the Nordic seas, releases heat to the atmosphere, and transforms into cold and dense waters that spill across gaps in the Greenland–Scotland Ridge as overflow plumes that feed the lower limb of the Atlantic meridional overturning circulation (AMOC). To better understand the overturning in the Nordic seas and the sensitivity of the AMOC to climate change, we need to understand where these dense water masses are formed and how they are delivered to the various overflow regions.

The origin of the largest overflow plume, which passes through the Denmark Strait on the western side of Iceland (e.g., Jochumsen et al. 2017), has been debated for several decades. While the primary source of the Denmark Strait Overflow Water (DSOW) was initially thought to be dense water formed by open-ocean convection in the Iceland and Greenland Sea gyres (Swift et al. 1980; Swift and Aagaard 1981; Strass et al. 1993), later studies argued that modified AW transported by the East Greenland Current (EGC) is the main source (Mauritzen 1996; Eldevik et al. 2009). In the latter scenario, the warm AW gradually cools and densifies as it follows the cyclonic circulation around the rim of the Nordic seas, and the two interior gyres contribute only to a limited extent. The Iceland Sea regained focus as a possible source of DSOW with the discovery of a
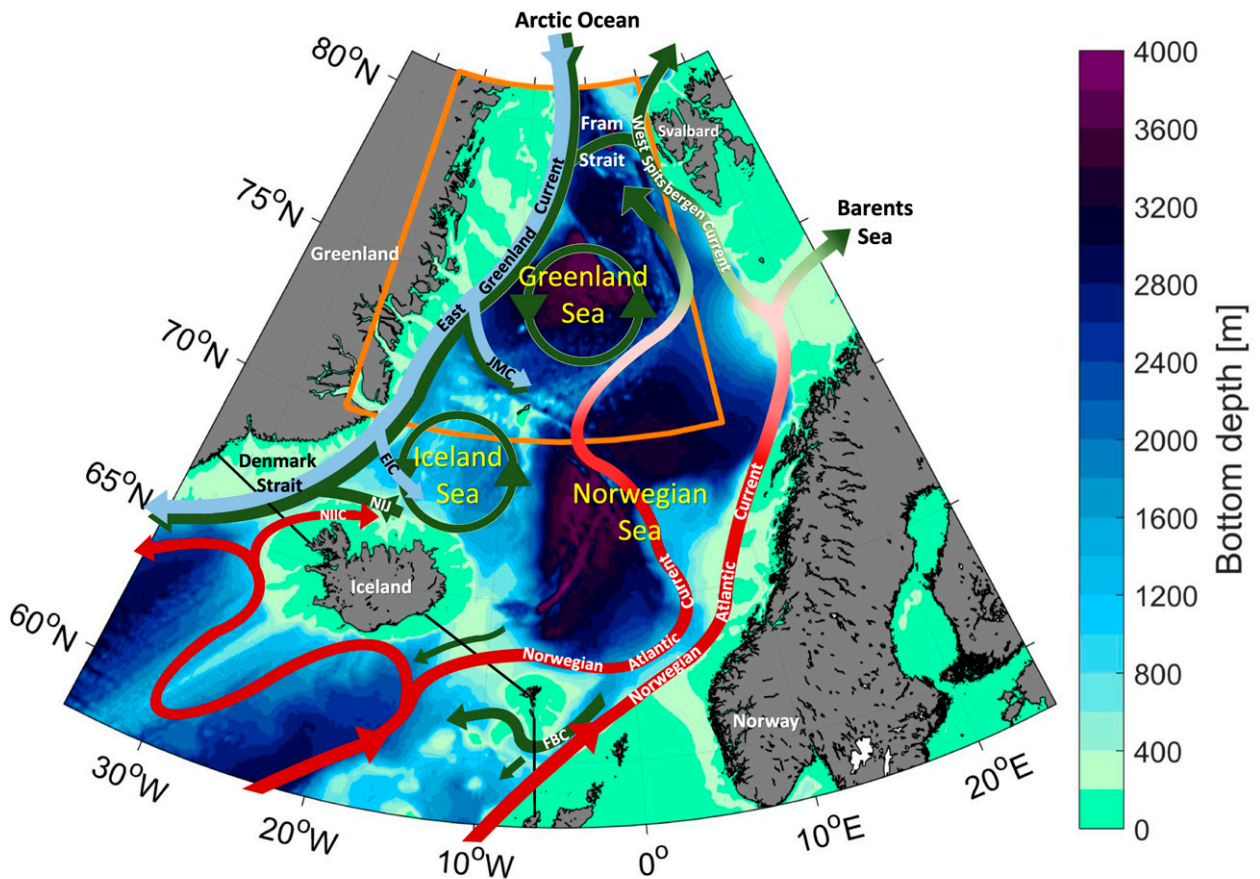

FIG. 1. Bathymetry and schematic circulation of the Nordic seas. Red arrows represent warm Atlantic water while dark green arrows indicate cold and dense waters. Fresh polar water is shown in light blue. The acronyms are the North Icelandic Irminger Current (NIIC), the North Icelandic Jet (NIJ), the East Icelandic Current (EIC), the Jan Mayen Current (JMC), and the Faeroe Bank Channel (FBC) overflow. The crest of the Greenland–Scotland Ridge is indicated by the black line. The orange box outlines the region of interest in this study.

current flowing along the continental slope north of Iceland toward the Denmark Strait, called the North Icelandic Jet (NIJ; Jónsson and Valdimarsson 2004). Recent estimates suggest that the NIJ supplies almost one-third of the DSOW and nearly all of the densest portion (with a potential density anomaly, referred to as potential density, larger than $28.03 \, \mathrm{kg \, m^{-3}}$; Våge et al. 2011), while the EGC accounts for the remaining part (Harden et al. 2016). Våge et al. (2011) hypothesized that the NIJ is the deep branch of a local overturning loop in the Iceland Sea that involves the boundary current system north of Iceland and water mass transformation in the interior Iceland Sea. However, Våge et al. (2015) and Pickart et al. (2017) later found that local convection in the Iceland Sea gyre may not be sufficient to provide all of the densest portion transported by the NIJ. They suggest instead that this dense water originates from the northwestern part of the Iceland Sea, where the deepest and densest

convection occurs, as well as from farther north in the Greenland Sea. A possible source in the Greenland Sea is supported by results from a tracer release experiment that demonstrate rapid communication of dense water from the Greenland Sea into the central Iceland Sea (Messias et al. 2008).

The largest overflow on the eastern side of Iceland, which passes through the Faeroe Bank Channel (FBC), accounts for approximately one-third of the total overflow water across the Greenland–Scotland Ridge (Østerhus et al. 2008; Hansen et al. 2016). According to Eldevik et al. (2009), more than 60% of the FBC overflow water originates from the Greenland and Iceland Seas. Fogelqvist et al. (2003) examined the composition of the FBC overflow using geochemical tracers. They concluded that the overflow water in the FBC is a mixture of about equal parts intermediate and deep water masses from the Norwegian Sea, and that the intermediate portion [Norwegian Sea Arctic

Intermediate Water (NSAIW)] is largely a product of wintertime convection in the Greenland Sea. By examining the evolution of the NSAIW, Jeansson et al. (2017) confirmed the importance of the Greenland and Iceland Seas, but they also revealed that a contribution from another, older water mass (upper Polar Deep Water formed in the Arctic Ocean) was required in order to explain the NSAIW properties. Although they argued that this water mass may be the largest source of the NSAIW, they also found that the proportion of intermediate waters formed in the Greenland Sea is increasing. The results of Jeansson et al. (2017) indicate a total supply from the Greenland Sea to the NSAIW of approximately 20%, but the contribution from the Greenland Sea at potential densities greater than $28.04 \, \mathrm{kg \, m^{-3}}$ was estimated to 50%. Thus, there is evidence that convection in the Greenland Sea may be important for the overflows both east and west of Iceland, in particular for waters denser than $28.03 \, \mathrm{kg \, m^{-3}}$, although the preferred pathways of the dense water are not fully known.

The convective activity in the Greenland Sea has changed extensively over the past decades. Early studies suggested that wintertime convection extended almost to the bottom, forming very cold and dense Greenland Sea Deep Water (GSDW; Helland-Hansen and Nansen 1909; Carmack and Aagaard 1973; Malmberg 1983; Aagaard et al. 1985). In winter 1971, Malmberg (1983) observed an oxygen-rich, nearly homogeneous layer extending from the surface to 3500 m in the center of the Greenland Sea, indicating convection nearly to the bottom. Since the late 1970s, however, convection has only been observed to intermediate ($<2000 \, \mathrm{m}$) depths, forming the slightly warmer and less dense Greenland Sea Arctic Intermediate Water (GSAIW; Meincke et al. 1992, 1997; Karstensen et al. 2005; Ronski and Budéus 2005; Latarius and Quadfasel 2010; Jeansson et al. 2017). Meincke et al. (1992) attributed the cessation of very deep convection to a combination of decreased cyclonic wind stress curl and reduced sea ice formation resulting in less brine release. The decreased wind forcing led to a weaker gyre circulation and increased intermediate stratification that isolated the cold GSDW dome from the surface. Recently, Moore et al. (2015) found that the magnitude of the atmospheric heat fluxes over the Greenland Sea have decreased by 20% since the end of the 1970s. They further suggested that if this trend continues, the mixed layer depth could be limited in the future such that only shallow convection occurs, which in turn could impact the production of dense water. However, the depth of convection also depends on the hydrographic conditions prior to the convective season. Lauvset et al. (2018) argued that increased salinity in the northward-propagating AW has increased the salinity and thereby decreased the stability of the upper 1500 m of the Greenland Sea water column since the early 2000s, which in turn has resulted in a tendency for deeper convection.

It is crucial to determine how various factors influence the depth of convection to fully understand the observed changes in the convective activity in the Greenland Sea and, furthermore, to shed light on its sensitivity to different conditions in the future. The main focus of the present study is to examine the interannual variability of convection and dense water formation in the Greenland Sea. Using a combination of hydrographic observations and a one-dimensional mixed layer model, we document the evolution of the convective product for the period 1986–2016 and explore its sensitivity to changes in hydrographic and atmospheric forcing conditions. In particular, we find that a new class of intermediate water started forming in the Greenland Sea gyre during the mid-1990s. We follow the evolution of this water mass and identify the main factors responsible for its development.

2. Data and methods

a. Hydrographic data

The hydrographic dataset used in this study includes measurements collected by shipboard conductivity, temperature, and pressure (CTD) instruments, autonomous profiling floats, and instrumented seals within the area outlined in orange in Fig. 1 over the time period 1986–2016. The shipboard CTD data were obtained from the archives of the Marine and Freshwater Research Institute of Iceland, the International Council for the Exploration of the Sea (ICES), the World Ocean Database, and the Norwegian Iceland Seas Experiment (NISE) database (Nilsen et al. 2008). Measurements from the autonomous profiling floats, which were first deployed in the Greenland Sea in 2001, were obtained from the archives of the international Argo program. We used delayed mode profiles that have been corrected for drift in salinity (by calibrating the float measurements against historical hydrography; Wong et al. 2003). The accuracy of the corrected float salinities are generally better than 0.01 (we use practical salinity throughout this study, which is nondimensional), while the temperature and pressure errors are less than 0.005°C and 2.4 dbar, respectively. The CTD profiles measured by instrumented hooded seals were postcalibrated against nearby Argo data [see Isachsen et al. (2014) for details on the data and calibration procedures]. The calibrated salinities have errors within the range 0.02–0.1, while the temperature measurements have an uncertainty of 0.03°C.
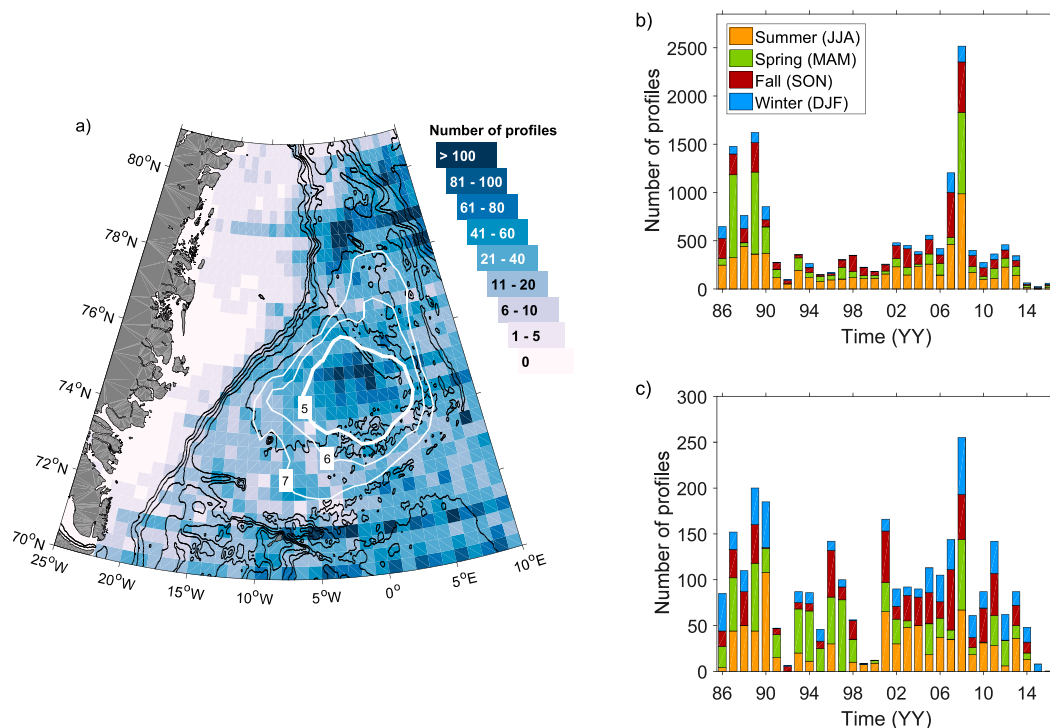
FIG. 2. (a) Total number of profiles per 1° longitude × 1/3° latitude bin, and number of hydrographic profiles per year, color coded by season, (b) for the entire domain and (c) inside the Greenland Sea gyre. The white contours in (a) indicate dynamic topography of the sea surface relative to 500-m depth (dynamic cm), and the thick white contour outlines the Greenland Sea gyre. The 500-, 1000-, 1500-, 2000-, 3000-, and 4000-m isobaths are marked in black.

Data from the various sources were combined into a single historical hydrographic dataset and quality controlled according to Skagseth and Mork (2012) and Våge et al. (2013, 2015). The procedure discards duplicates, erroneous profiles, and outliers. Measurements with temperature and salinity values outside the expected range in the Nordic seas of [−2°, 20°C] and [20, 36], respectively, were not included. Neither were profiles with density inversions exceeding 0.05 kg m^{-3} except when the inversion was a single data spike, in which case the spike was removed. Outliers were identified by comparing each profile to all other profiles within an effective radius of 110 km (Davis 1998; Våge et al. 2013). The effective radius was increased along isobaths, resulting in an anisotropic area of comparison where the magnitude of the elongation was set by the difference in bottom depth across the topography. This procedure was used because currents in the Nordic seas tend to follow the topography, resulting in smaller variations in hydrography along than across topographic gradients (e.g., Nøst and Isachsen 2003). All profiles within the effective radius were interpolated onto a common vertical coordinate at 5-m intervals and the profile in question was considered an outlier if it

contained data points that differed from the mean temperature and salinity, at any depth, by more than six standard deviations.

The spatial and temporal distributions of the data are shown in Fig. 2. The thick white contour in Fig. 2a outlines the cyclonic gyre in the Greenland Sea defined according to Moore et al. (2015) by the dynamic topography of the sea surface relative to 500-m depth. The center of the cyclonic gyre was identified by the minimum in dynamic topography. A closed contour around this minimum was then chosen as the gyre boundary such that a sufficiently large number of homogeneous profiles were included. While the geographical data coverage is quite good, apart from the Greenland shelf, there are temporal biases (Figs. 2b,c). Wintertime observations are generally scarce because of harsh weather conditions and the presence of sea ice. The deepest convection occurs at the end of winter (February–April; Våge et al. 2015; Marnela et al. 2016). However, less than 20% of the profiles were obtained at this time of the year. We also note that most of the data from the Greenland Sea gyre were obtained by Argo floats, which results in a denser coverage after 2001. The majority of the CTD data collected by the instrumented

seals are located along the Greenland shelf, where data from other sources are sparse. All of these profiles were obtained during 2007–2008. The vertical resolution of the hydrographic profiles differs for each data source, measurement method, and with time, but is generally within the range 1–50 m.

b. Mixed layer depths

The depths and hydrographic properties of the mixed layer were determined following a robust procedure used by Våge et al. (2015) for the Iceland Sea that involves visual inspection of each hydrographic profile. Two independent automated routines, one based on a density-difference criterion (Nilsen and Falck 2006) and one based on the curvature of the temperature profile (Lorbacher et al. 2006), were used to estimate the vertical extent of the mixed layer (see appendix A for further details). By visual inspection, we found that at least one of the two automated routines accurately determined the mixed layer depth for 61% of the profiles. A manual routine developed by Pickart et al. (2002) was employed for the remaining profiles (appendix A).

The automated routines were less accurate for profiles with small density gradients between the mixed layer and the deeper part of the water column, which is typical for wintertime profiles in the Greenland Sea. Several profiles also had a mixed layer that was separated from the surface, because of early stages of restratification in the surface layer or in the form of multiple stacked mixed layers, that the automated routines were not able to identify. Such isolated mixed layers have also been observed during periods of active convection in the Irminger, Iceland, and Labrador Seas (Våge et al. 2009, 2015; Pickart et al. 2002).

c. Gridding of the hydrographic data

To investigate the lateral distribution of a given property, the data were interpolated onto a regular 0.5° longitude × 0.2° latitude grid. The value of each grid point was found from the average (weighted by the inverse distance) of all measurements within an effective radius $r = 50$ km, which was increased along isobaths to account for the greater correlation length scales along topography (Skagseth and Mork 2012; Våge et al. 2013). To study the temporal evolution of the water column in the central Greenland Sea, we interpolated profiles within the gyre onto a regular time versus depth grid of 14 days by 50 m. All data points within the gyre were first assigned to their nearest grid point and, if several data points were allocated to the same grid point, an average value was estimated. Interpolation was then performed by fitting a Laplacian-spline surface to this new partly gridded dataset (Pickart and Smethie 1998). The resulting

gridded product was finally smoothed by convolution with a Gaussian window of 42 days by 150-m depth.

d. Atmospheric forcing

Atmospheric fluxes were obtained from ERA-Interim (ERA-I herein), which covers the period from 1979 to the present (Dee et al. 2011). The parameters included in this study are the 6-hourly air–sea fluxes of heat, freshwater, and momentum, as well as the sea ice concentration. The ERA-I longwave radiative heat flux from the ocean to the atmosphere is known to be underestimated at high latitudes by approximately 20–30 W m^{-2} because of biases in the cloud parameterization (Walsh et al. 2009; Chaudhuri et al. 2014). To account for this underestimation, we followed Moore et al. (2015) and added a constant offset of 25 W m^{-2} to the longwave heat flux. The atmospheric fluxes were averaged over the area of the Greenland Sea gyre outlined in Fig. 2a. When sea ice was present in the gyre, we estimated the ocean–atmosphere turbulent heat flux Q_{thf}^{ocean} (latent and sensible heat fluxes) according to Moore et al. (2015) as

$$Q_{thf}^{ocean} = \frac{Q_{thf} - A Q_{thf}^{ice}}{1 - A} \approx \frac{Q_{thf}}{1 - A}, \qquad (1)$$

where Q_{thf} is the total turbulent heat flux obtained from ERA-I and A is the mean sea ice concentration over the gyre. It is assumed that the total turbulent heat flux over the ice-covered region Q_{thf}^{ice}, which is typically an order of magnitude lower than over open water, can be neglected.

e. One-dimensional mixed layer model

The so-called Price-Weller-Pinkel (PWP) one-dimensional mixed layer model (Price et al. 1986) was employed in order to investigate the sensitivity of the mixed layer development in the Greenland Sea to various hydrographic and atmospheric forcing conditions (see appendix B for details). As atmospheric forcing, we applied the ERA-I heat, freshwater, and momentum fluxes averaged over the area of the Greenland Sea gyre, and as initial conditions, we used mean fall (October–November) hydrographic profiles. The model was set up with a vertical resolution of 2 m and with 6-hourly time steps.

Moore et al. (2015) recently modified the PWP model for the Greenland Sea gyre to include lateral advection of heat, which is necessary in order to balance the annual heat budget. We further parameterized lateral advection of salt in the present model version to obtain balanced freshwater budgets. A detailed description of the parameterization is given in appendix Bb. Production of sea ice was also included in the present model version because brine release
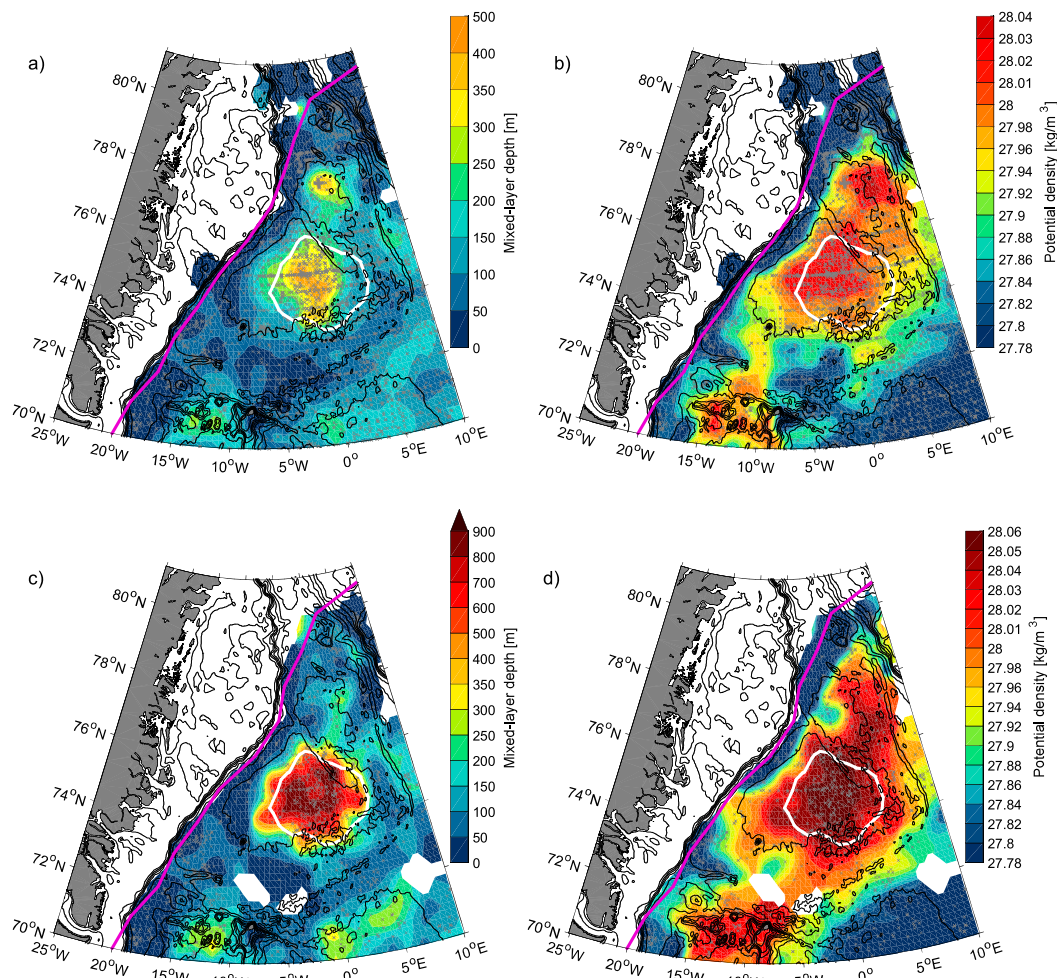
FIG. 3. Mean late-winter (February–April) (a) mixed layer depth and (b) potential density from 1986 to 2016 and the (c),(d) corresponding maps for winters with mean convection depth exceeding the 70th percentile. The locations of data points are indicated by gray crosses. The 200-, 400-, 600-, 800-, 1000-, 1400-, 2000-, 3000-, and 4000-m isobaths are shown as thin black lines. The white contour outlines the Greenland Sea gyre and the magenta curve denotes the mean 50% sea ice concentration contour during November–April.

by sea ice formation has been considered one of the main drivers for deep convection in the Greenland Sea (e.g., Visbeck et al. 1995; Marshall and Schott 1999). Estimation of sea ice production and the resulting salt flux are described in appendix Bc. We note, however, that there was hardly sea ice within the gyre during the time period covered here [except the winters between 1986 and 1990 and in 1997–98; see Fig. 2b in Moore et al. (2015)].

3. Greenland Sea mean late-winter mixed layer properties

Mean late-winter (February–April) mixed layer depth and potential density from 1986 to 2016 are shown in Figs. 3a and 3b. The deepest and densest mixed layers were located near the center of the

Greenland Sea gyre where the cyclonic circulation weakens the stratification, preconditioning the gyre for deep convection compared to the more stratified surrounding waters (Marshall and Schott 1999). A region of relatively deep convection is visible also in the Boreas Basin near 78°N where another, smaller cyclonic gyre has been observed (Quadfasel and Meincke 1987). However, as the majority of the measurements in this area were obtained in winter 1993/94, it is difficult to say whether this local maximum is a recurring feature.

Regions with high mixed layer density (above $28.01 \, \mathrm{kg \, m^{-3}}$) were observed both in the central Greenland Basin and in the Boreas Basin as well as farther south in the Iceland Sea. Våge et al. (2015) found that the deepest and densest mixed layers in the

Iceland Sea are located in the northwest corner, on the outskirts of the gyre, even though the center of the gyre is more preconditioned for convection. They argue that this is due to the stronger atmospheric fluxes near the ice edge. While stronger heat fluxes also occur close to the ice edge in the Greenland Sea (Papritz and Spengler 2017), the deepest mixed layers there are largely confined to the area of the cyclonic gyre. This difference could be a result of the weaker stratification or the generally higher heat fluxes in the Greenland Sea gyre compared to the Iceland Sea gyre (Marshall and Schott 1999; Moore et al. 2015). According to Moore et al. (2015) the winter-mean turbulent heat flux within the Iceland Sea gyre ranged from 50 to $100 \, W \, m^{-2}$, while the heat flux in the central Greenland Sea has been within the range $100–150 \, W \, m^{-2}$ over the time period 1986–2015 (Fig. 4d).

The mean depth of the late winter mixed layer in the Greenland Sea gyre is approximately 500 m (Fig. 3a). However, the interannual variability of both the mixed layer depth and properties is substantial. By including only winters of deep convection (in which the mixed layer depth within the gyre exceeded the 70th-percentile value; Figs. 3c,d), we found that the mean mixed layer in the center of the gyre exceeded 800 m. During these winters, mixed layer densities greater than $\sigma_\theta = 28.03 \, kg \, m^{-3}$ were observed over a considerably larger area.

4. Temporal variability of the mixed layer in the central Greenland Sea

The temporal variability of the mixed layer was examined in detail within the Greenland Sea gyre (hereafter referred to as the Greenland Sea), where the deepest and densest convection occurs. The evolution of mean late-winter mixed layer depth and density from 1986 to 2016 are shown in Fig. 4 (only the 50% deepest mixed layers were included in order to exclude restratified profiles and profiles that were obtained before the onset of deep convection). Apart from one winter prior to 1993 (1988/89), the average mixed layer did not extend deeper than 200–300 m. In this period, the coldest, least saline, and least dense mixed layers were observed (mixed layer temperature and salinity are not shown). After 1993, mixed layer depths have in general exceeded 500 m with few exceptions, while sufficiently dense water ($\sigma_\theta > 28.03 \, kg \, m^{-3}$) to supply the densest portion of the NIJ, and hence also of the DSOW (Våge et al. 2011; Mastropole et al. 2017) has regularly been produced in the center of the Greenland Sea. Such dense waters are probably not formed in large amounts in the Iceland Sea (Våge et al. 2015).
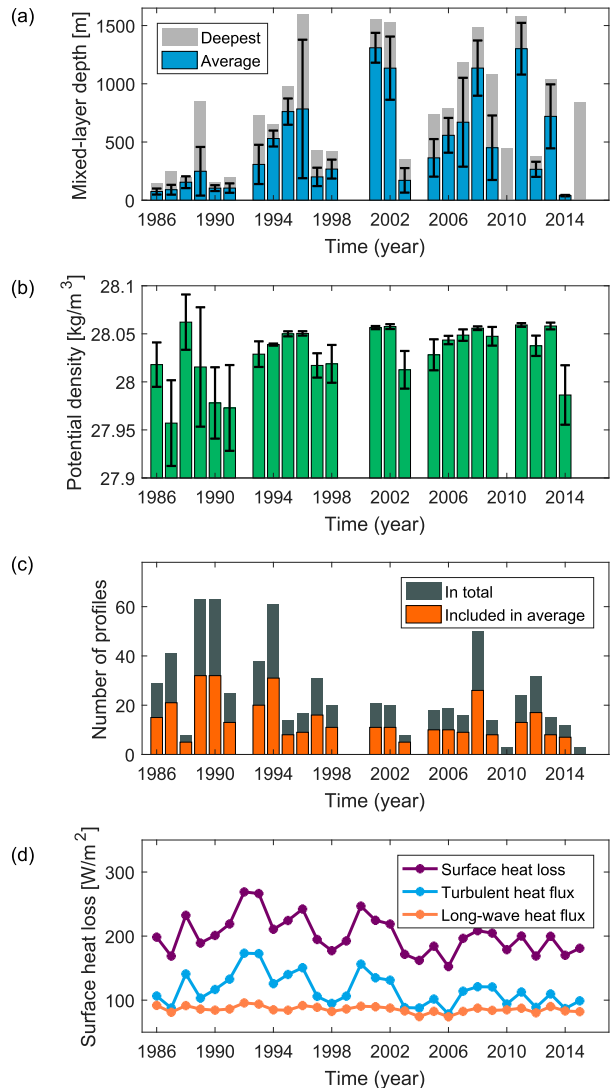

FIG. 4. Mean late-winter (February–April) (a) mixed layer depth and (b) potential density in the Greenland Sea from 1986 to 2016 (colored bars). The black error bars indicate one standard deviation. Average values were excluded for winters with fewer than five profiles (2010 and 2015). The deepest mixed layer observed each winter (light gray bars) is also shown in (a). (c) The total number of profiles each winter (gray) and the number of profiles included in each average (orange). (d) The winter-mean (November–April) surface heat loss (sum of turbulent and longwave heat fluxes). Positive values denote heat loss to the atmosphere.

The temporal evolution of the hydrographic properties of the upper 2000 m of the Greenland Sea are shown in Fig. 5. The upper 500 m of the water column are largely dominated by the seasonal cycle. Several salinity minima are, in addition, visible close to the surface. The two prominent minima that took place in the time periods 1986–93 and 1996–98 coincide with the Great Salinity Anomalies reported by Belkin et al. (1998)
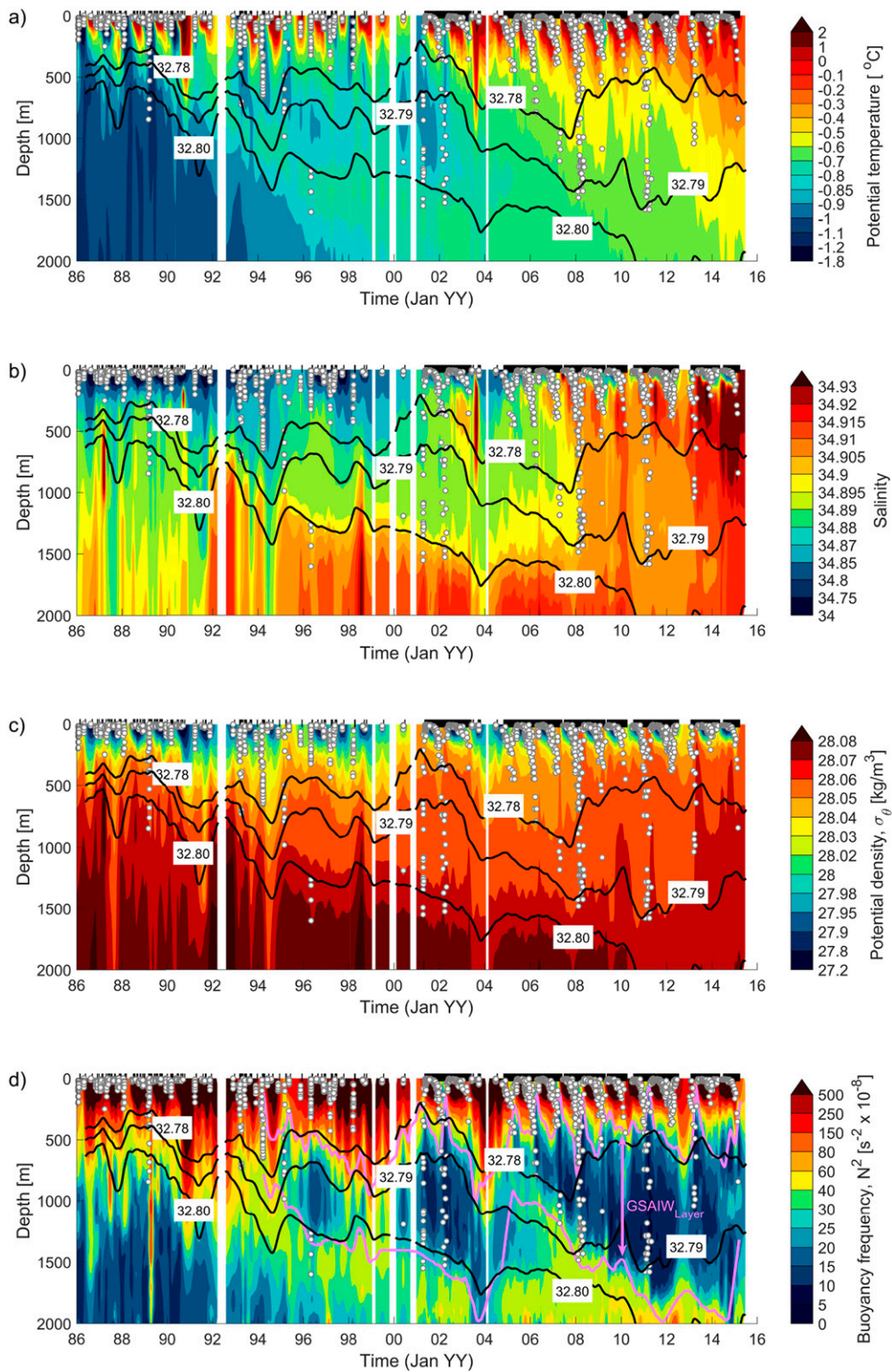
FIG. 5. Evolution of (a) potential temperature, (b) salinity, (c) potential density, and (d) buoyancy frequency within the upper 2000 m of the Greenland Sea gyre from 1986 to 2016. The white dots show the mixed layer depth for each in situ profile, and the black bars along the top of the figures indicate the time of each profile. The black contours represent σ_1 levels equal to 32.78, 32.79, and 32.80 kg m^{-3}. The magenta contours in (d) illustrate the extent of the GSAIW layer.
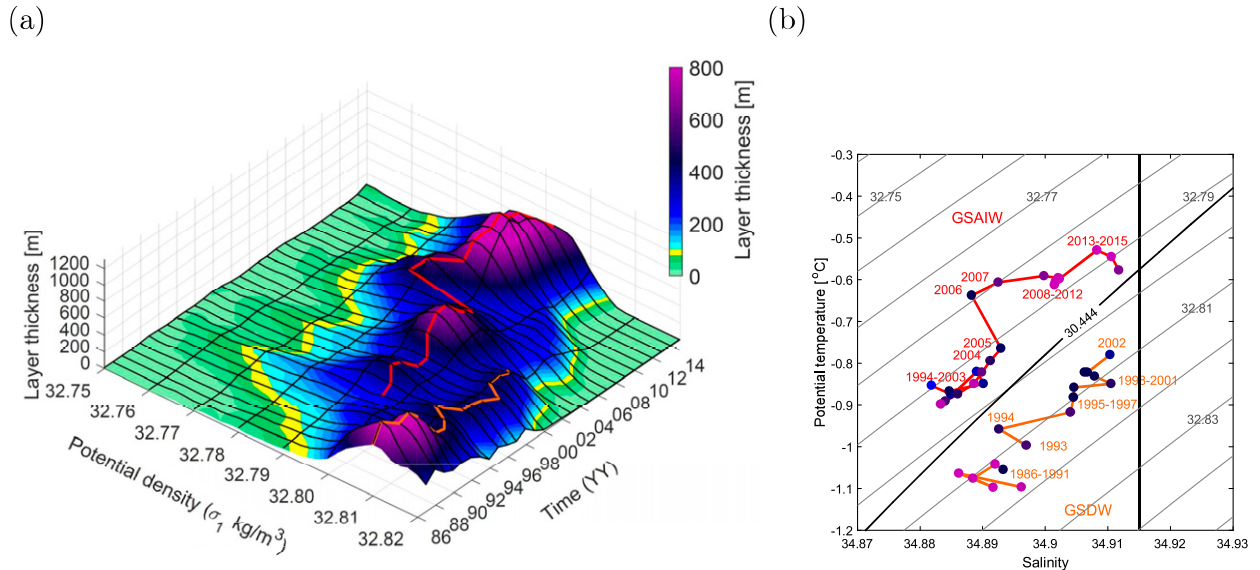
(a)

(b)

FIG. 6. (a) Temporal evolution of annual-mean thickness of $\Delta\sigma_1 = 0.01\,\mathrm{kg\,m^{-3}}$ layers within the upper 2000 m of the Greenland Sea from 1986 to 2015. The marked σ_1 values are the center values for each density layer. For the construction of this plot, σ_1 layers overlapping by $0.002\,\mathrm{kg\,m^{-3}}$ have been used. The red and orange lines follow the maximum layer thickness associated with the GSAIW and GSDW, respectively. (b) The corresponding annual-mean potential temperature and salinity characteristics of the GSAIW and GSDW. The colors of the dots correspond to the layer thickness in (a), and the gray lines are σ_1 contours. Following Rudels et al. (2005), we define GSDW by $\sigma_{0.5} \geq 30.444\,\mathrm{kg\,m^{-3}}$ and salinity $S \leq 34.915$ (marked by the black lines), and GSAIW by $\sigma_\theta \geq 27.97\,\mathrm{kg\,m^{-3}}$, $\sigma_{0.5} \leq 30.444\,\mathrm{kg\,m^{-3}}$, and potential temperature $\Theta \leq 0^\circ$C.

and Belkin (2004), respectively. Another less pronounced freshwater anomaly occurred between 2003 and 2005.

The hydrographic variability below 500 m is characterized by interannual changes in wintertime convection and by long-term trends. A substantial warming and salinification of the upper 1500 m of the water column has taken place over the past three decades (Figs. 5a,b). The salinity increase has been particularly strong over the last 15 years. This corroborates the results of Lauvset et al. (2018), who further argue that the increasing salinity has decreased the stratification of the upper 2000 m and thereby preconditioned the Greenland Sea for deeper convection compared to the 1990s. In the early 1990s, at around 400–600-m depth, we can see the development of the intermediate temperature and stratification maxima documented by, for example, Karstensen et al. (2005) and Latarius and Quadfasel (2010). Both maxima gradually descended until 2004 (following the isopycnal $\sigma_1 = 32.80\,\mathrm{kg\,m^{-3}}$; see Figs. 5a,d). Thereafter, the temperature maximum vanished, while another intermediate stability maximum [also noted by Marnela et al. (2016)] occurred between 2004 and 2008. The deepening of the stability maxima is associated with periods of strong wintertime convection, which results in an increased volume of weakly stratified water (Fig. 5d). In the following sections, we investigate the evolution of these weakly stratified waters in order to better understand the water mass transformation that takes place in the central Greenland Sea.

5. A new class of GSAIW

The evolution of the water masses formed within the central Greenland Sea was examined using a volumetric approach (e.g., Yashayaev et al. 2007). Annual mean density profiles were first calculated for each year in order to remove the seasonal cycle and focus on interannual and longer-term changes. For each profile, we then estimated the thickness of different potential density layers ($\Delta\sigma_1 = 0.01\,\mathrm{kg\,m^{-3}}$) overlapping by $0.002\,\mathrm{kg\,m^{-3}}$. We used the potential density anomaly referenced to 1000 m (i.e, σ_1) since it better resolves the density changes where the intermediate water masses that are the main product of convection are located. The distance between the various σ_1 isopycnals closely follows the development of the weakly stratified layers as shown by the black contours in Fig. 5d (increases in layer thickness correspond to periods of enhanced dense water production).

The resulting distribution of layer thickness (Fig. 6a) illustrates the evolution of the various classes of water formed in the Greenland Sea. The maximum in layer thickness present before 1990 at a potential density of approximately $32.81\,\mathrm{kg\,m^{-3}}$ indicates the cold and
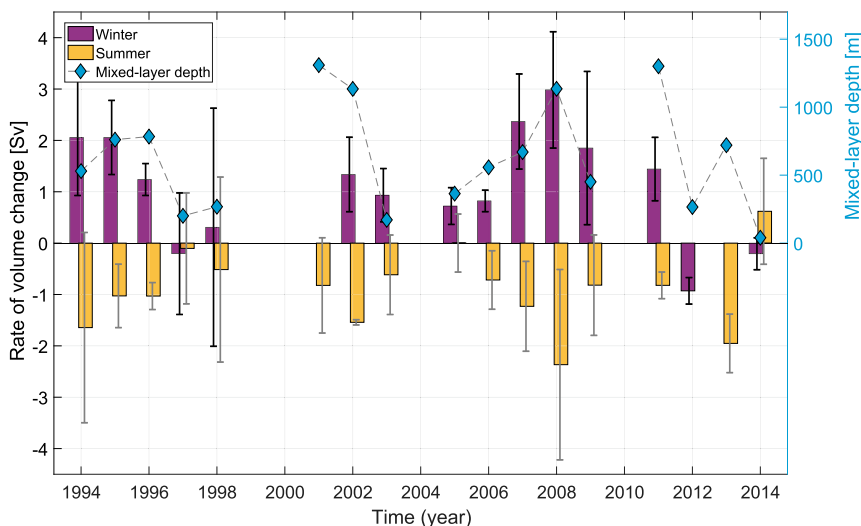
FIG. 7. Average rate of volume change of the GSAIW layer through each winter (purple bars) and summer (yellow bars) since 1994. The winter rates were estimated based on the change in volume over the 6-month period from fall (September–November) to spring (March–May), while the summer rates were based on the change in volume from spring to fall. Average values were excluded for winters/summers with fewer than five profiles in fall or spring. The error bars indicate one standard deviation, and the light blue diamonds mark the mean late-winter (February–April) mixed layer depth.

relatively fresh GSDW that occupied most of the water column below 500 m. The volume of GSDW then gradually decreased until 2002 because of limited ventilation before it vanished from the upper 2000 m of the water column. In 1994/95, another less pronounced maximum appeared, corresponding to the development of a new, less dense class of intermediate water. These years were also the first, since the beginning of this record, with mean late-winter mixed layer depths exceeding 500 m (Fig. 4a). Although the new class of intermediate water (GSAIW) started forming while remnants of the GSDW were still present in the upper 2000 m of the water column, they were separated by the intermediate temperature and stability maxima (Figs. 5a,d). The amount of GSAIW formed after 1994 varied significantly from year to year depending on the depth and intensity of convection. Substantial formation took place in years with relatively deep convection, such as 2002, 2008, and 2011. Periods of limited renewal coincided with the shallow convective years of 1996–98 and 2003–05. The overall proportion of the water column occupied by the homogeneous GSAIW has increased since 1994. It is presently the dominant water mass of the upper 2000 m of the Greenland Sea. The red and orange lines in Fig. 6a follow the maximum layer thicknesses associated with the GSAIW and GSDW, respectively. The corresponding temperature and salinity time series shown in θ–S space in Fig. 6b demonstrate that

the temperature and salinity of both water masses have increased through the record. In terms of density, however, the overall effect is small, as the temperature and salinity changes largely compensate.

We have shown that the volume of GSAIW has increased substantially since the new class first started forming in winter 1994. To examine the rate of production and export each year, we estimated seasonal changes in the volume of the GSAIW layer following the method of Yashayaev and Loder (2016). The mean volume of GSAIW was first estimated each fall (September–November) and spring (March–May). Then we calculated the volume change through each winter and summer and divided by 6 months (assuming constant rate of change through each period). The average rates of volume change (including one standard deviation) from 1994 to 2014 are shown in Fig. 7. Positive values mean that the volume of the GSAIW increased. The definition of the GSAIW layer (illustrated in Fig. 5d) was based on the center σ_1 value $(\pm 0.01 \, \mathrm{kg \, m^{-3}})$ of the density layer with maximum layer thickness at the end of each winter (April–May). The development of this layer captures the evolution of the main water mass produced inside and exported out of the Greenland Sea gyre each year. More than 87% of the profiles that indicate ventilation of the GSAIW layer were located within the Greenland Sea gyre. We note, however, that this definition does not include all waters ventilated in the Greenland Sea that are sufficiently dense

$(\sigma_\theta > 27.8 \, \mathrm{kg \, m^{-3}})$ to potentially contribute to the overflow waters. In particular, it excludes the least dense waters in this range that are also formed in areas surrounding the gyre (see Figs. 3b,d).

The average rate of volume change of the GSAIW layer through winter, over the 6-month period from fall to spring (purple bars in Fig. 7), is larger during winters of deep convection as more GSAIW is produced. These GSAIW production estimates are biased low because of the unaccounted export that also takes place throughout winter. For some of the shallow convective winters, the rate of change is negative. This simply means that the export of GSAIW exceeds the production. The minimum rate of wintertime production required to explain the observed volume changes (which would be zero for the shallow convective winters with negative rates) is 1.2 ± 0.9 Sv (1 Sv ≡ $10^6 \, \mathrm{m^3 \, s^{-1}}$) averaged over the time period 1994–2014. This equals an annual production of 0.6 ± 0.5 Sv if we assume zero formation in summer.

The rates of volume change through summer (over the 6 months from spring to fall, shown by the yellow bars in Fig. 7) may be interpreted as the net export (sum of total import and export) out of the Greenland Sea gyre during summer. Since the net export includes possible import into the gyre, it must be less than the total export of GSAIW. The positive rate in 2014 is most likely an artifact of spatial differences within the gyre. That year there were relatively few observations, and all March–May profiles were clustered in the southwest corner of the gyre, while almost every September–November profile was located in the northern part of the gyre. The average summer net export, excluding 2014, is 0.9 ± 0.7 Sv. This is within the transport range (0.2–0.9 Sv) presented by Karstensen et al. (2003) for the 1990s. Our estimate is lower than the value found by Messias et al. (2008), who inferred an export rate of 1–1.85 Sv from a tracer study. A reason for this discrepancy may be that their estimate was based on data surrounding the central Greenland Sea in the time period 1998–2002, during which we have only a limited amount of data from within the gyre. The rates of export and production are also highly variable. The largest summertime exports generally follow winters with deep convection. Because of this large variability, we have not made an attempt at estimating wintertime and annual export rates.

6. Mechanisms controlling the interannual variability of the Greenland Sea water mass transformation

To investigate the variability of the water mass transformation in the Greenland Sea and to explore why the new class of intermediate water started

TABLE 1. Mean atmospheric forcing (November–April) from 1986 to 2015 used in the PWP model simulations. The turbulent heat flux (latent and sensible heat fluxes) used in the various model simulations span the range 30–880 W m^{-2}, while the overall winter-mean turbulent heat flux was 125 W m^{-2}. Positive fluxes are directed out of the ocean.

Term	Value
Atmospheric freshwater flux	$2.7 \times 10^{-9} \, \mathrm{m \, s^{-1}}$
Surface solar radiation	$-27 \, \mathrm{W \, m^{-2}}$
Surface thermal radiation	$112 \, \mathrm{W \, m^{-2}}$
Latent heat flux	$59 \, \mathrm{W \, m^{-2}}$
Sensible heat flux	$66 \, \mathrm{W \, m^{-2}}$
Wind stress τ_x	$0.01 \, \mathrm{N \, m^{-2}}$
Wind stress τ_y	$0.08 \, \mathrm{N \, m^{-2}}$

forming in 1994/95, we employed the PWP mixed layer model described in section 2e (details are given in appendix B). Idealized model runs were conducted for a range of initial and atmospheric forcing conditions to shed light on the most important factors regulating the observed mixed layer variability in the Greenland Sea. Lateral advection of heat and salt are also important for setting the properties of the mixed layer. They were parameterized as described in appendix B (section b) and assumed constant in all model runs.

The influence of the various atmospheric forcing components on the mixed layer development was explored by sensitivity studies using the PWP model. As expected from previous work (e.g., Våge et al. 2008; Moore et al. 2015), we found that the most important component was the turbulent heat flux (not shown). The remaining air–sea fluxes were therefore kept constant in all model runs equal to the overall winter-mean values from 1986 to 2015 (Table 1). We applied constant forcing through winter from November to April in each simulation, and the span of winter-mean turbulent heat fluxes explored was based on the range of observed values over the 1986–2015 period. We ran the model for winter-mean turbulent heat fluxes equal to every 5th percentile of all winter values. To generate idealized initial conditions, we estimated the convection resistance (CR) of every hydrographic profile in fall (October–November). CR is an integral measure of the density stratification and was computed following Frajka-Williams et al. (2014) as

$$\mathrm{CR}(h) = \int_{-h}^{0} \sigma_1(S, \theta, z) \, dz - h\sigma_1(S, \theta, h), \qquad (2)$$

where S, θ, z, and σ_1 are the salinity, potential temperature, depth, and the potential density anomaly referenced to 1000 m, respectively. We chose $h = 1000$-m

depth since this is where the core of the GSAIW is located. The fall profiles were then sorted according to CR and initial conditions were determined as the mean over every 5th percentile.

The resulting end-of-winter mixed layer depths as a function of convection resistance and surface heat loss (sum of turbulent and longwave heat fluxes) are shown by the background color in Fig. 8a. The colored dots indicate the observed mean late-winter mixed layer depths each winter. Although the model underestimates the mixed layer depth slightly, the observations are generally in good agreement with the model results, with deeper mixed layers occurring when heat loss is high and stratification is weak. The contribution of brine release by sea ice formation to the mixed layer deepening is illustrated in Fig. 8b. Conditions required to form sea ice (strong stratification and high surface heat loss) were absent during most of the time period covered by our study. Sea ice formation contributed to a deepening of the mixed layer in 1988, 1989, 1992, and 1993, but the effect was not sufficiently large to result in convection exceeding 400 m.

From 1993 to 1994, a remarkable decrease in stratification took place. The concurrent decrease in heat loss suggests that the change in stability was the primary factor leading to the deeper mixed layers and the formation of the new class of intermediate water in winter 1993/94. A further decrease in stratification resulted in continued ventilation of the new GSAIW until 1996 (the evolution is marked by the black dashed line in Fig. 8a).

To determine the cause of the remarkable decrease in stratification from 1993 to 1996, we examined the evolution of the hydrographic properties in the upper 50 m of the water column. Interannual variability in mixed layer density and, in turn, depth were generally dominated by changes in mixed layer salinity. Shallow convection was associated with cold and fresh mixed layers, while deep convection coincided with warmer and more saline mixed layers (not shown). Earlier studies have also noted the connection between the near-surface salinity and the depth of the mixed layer (e.g., Ronski and Budéus 2005; Latarius and Quadfasel 2010). Examining the 1986–2016 period, we find that when the near-surface salinity in summer was lower than the mean value of 34.71, and the late winter mixed layer depths generally did not exceed 300 m (negative anomalies in Fig. 9). Thus, it appears that there is a threshold beneath which the fresh surface layer will inhibit convection, regardless of the magnitude of the surface heat loss (shown in colors). A similar example from the Labrador Sea is the shallow convection (100–200 m) observed during the Great Salinity Anomaly between 1969 and 1971 (Lazier 1980). In this case, the shutdown of
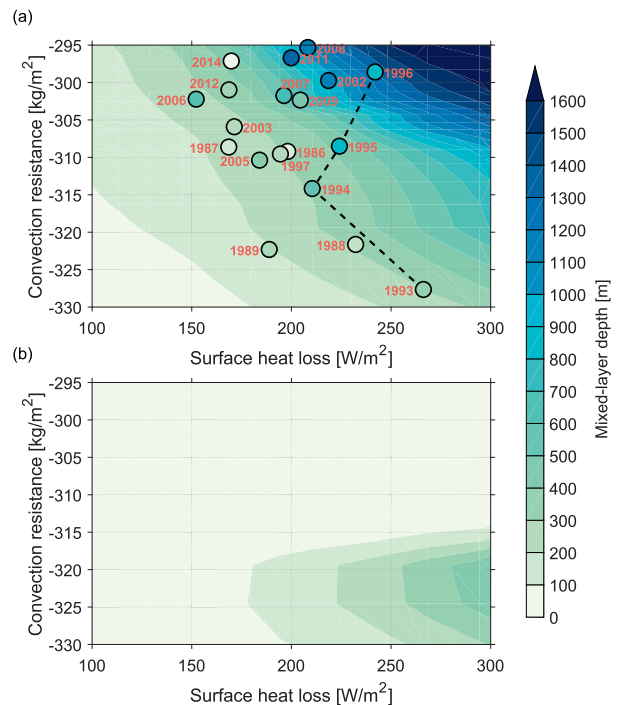

FIG. 8. (a) Simulated end-of-winter mixed layer depth (background color) as a function of winter-mean surface heat loss (turbulent and longwave heat fluxes) and convection resistance. Convection resistance is a measure of the mean fall (October–November) stratification. More-negative values indicate stronger stratification. The colored circles show observed mean late-winter (February–April) mixed layer depths and the black dashed line indicates the change in stratification over the time period 1993–96 prior to and during the formation of the new class of GSAIW. (b) The contribution from sea ice formation to the deepening of the mixed layer, that is, the difference between simulated mixed layer depths using the full model and simulations excluding brine release by sea ice formation.

deep convection resulted from a combination of low near-surface salinity and weak atmospheric forcing (Gelderloos et al. 2012). The shallow convective winters 1988–93 in the Greenland Sea were, however, among the most severe winters in terms of atmospheric heat loss (see Figs. 8, 9). The winter-mean buoyancy flux between 1988 and 1993 (estimated following Gelderloos et al. 2012) was also 1.15 times larger than the winter-mean buoyancy flux in 1994–96 when the new class of intermediate water started forming. This suggests that the low-salinity layer stratifying the upper part of the water column was the main reason for the shallow convection prior to 1993. The effect of sea ice formation was too weak to compensate for the strong stratification generated by the fresh surface layer.

The decrease in water-column stability from 1993 to 1996 resulted from a substantial increase in salinity (black dashed line in Fig. 9). The weaker stratification
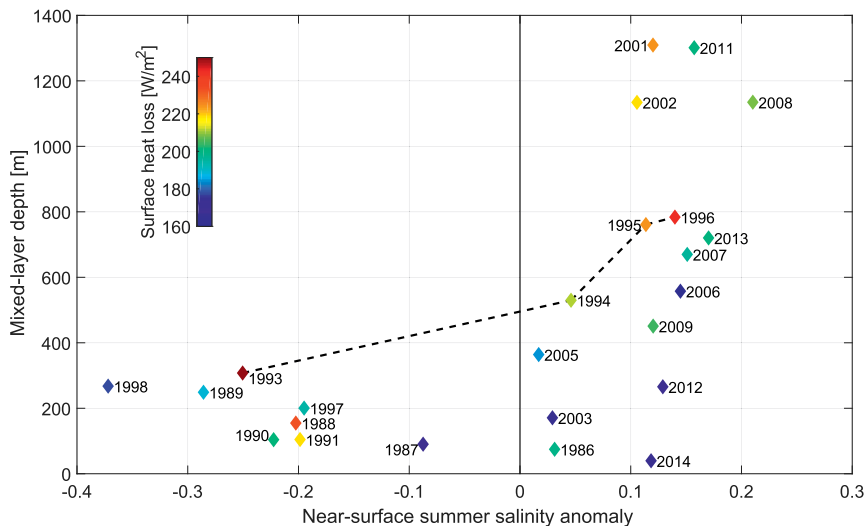
FIG. 9. Mean late-winter (February–April) mixed layer depths vs mean summer (June–October) near-surface (0–50 m) salinity anomalies from 1985 to 2015. The mean near-surface salinity over the entire time period was approximately 34.71 (indicated by the vertical black line). Winter-mean surface heat loss (turbulent and longwave heat fluxes) is shown in color. The black dashed line marks the evolution from 1993 to 1996 when the new class of GSAIW started forming.

along with sufficiently strong atmospheric forcing set the stage for the formation of the new class of intermediate water. The near-surface salinity anomaly has remained positive after 1994 (except for the 1997–98 period), which is required for the continued ventilation of the intermediate water mass. The winters with deepest convection were characterized by both high near-surface salinities in fall and strong atmospheric heat loss through winter.

7. Concluding remarks

We utilized hydrographic data from several archives including measurements from ships, autonomous profiling floats, and instrumented seals to examine the convective activity in the Greenland Sea over the period 1986–2016. By estimating the mixed layer depth for each hydrographic profile, using a robust procedure involving visual inspection, we found that the deepest and densest mixed layers in the Greenland Sea took place in late winter (February–April) and were located within the cyclonic gyre. Although convection was confined to intermediate depths (<2000 m) during the entire period, the late winter mixed layer depth and the resulting dense water product exhibited large interannual variability. Particularly interesting was the transition from predominantly shallow convection (<300 m) in 1988–93 to the relatively deep convection (500–1000 m) observed in winters 1994–96. This transition marked the beginning of the formation

of a new, less dense class of intermediate water, which since 1994 has been the main product of convection in the Greenland Sea.

The relative importance for this transition of various factors such as sea ice formation, atmospheric heat loss, and stability of the water column were explored using a one-dimensional mixed layer model within a parameter space representative for the Greenland Sea. Sea ice formation contributed to a slight deepening of the mixed layer in four winters in the late 1980s and early 1990s, but was not a main forcing mechanism for the convective activity in the Greenland Sea during the time period covered by our study (1986–2016). The shallow convection in 1988–93 resulted from a near-surface freshening that increased the stability of the upper part of the water column. These winters were also accompanied by strong atmospheric forcing, which suggests that the main factor limiting convection was the increased near-surface freshwater content.

Possible sources of freshwater to the Greenland Sea are precipitation and inflow of ice and low-salinity water from the EGC. Aagaard and Carmack (1989) estimated the excess precipitation to account for only 9% of the annual freshwater addition to the Greenland Sea, and Latarius and Quadfasel (2016) found, from budget calculations, that the atmospheric freshwater flux is around two orders of magnitude lower than the lateral input. This implies that freshwater input from the EGC is the dominant source of freshwater to the Greenland Sea. The amount of freshwater transported southward from
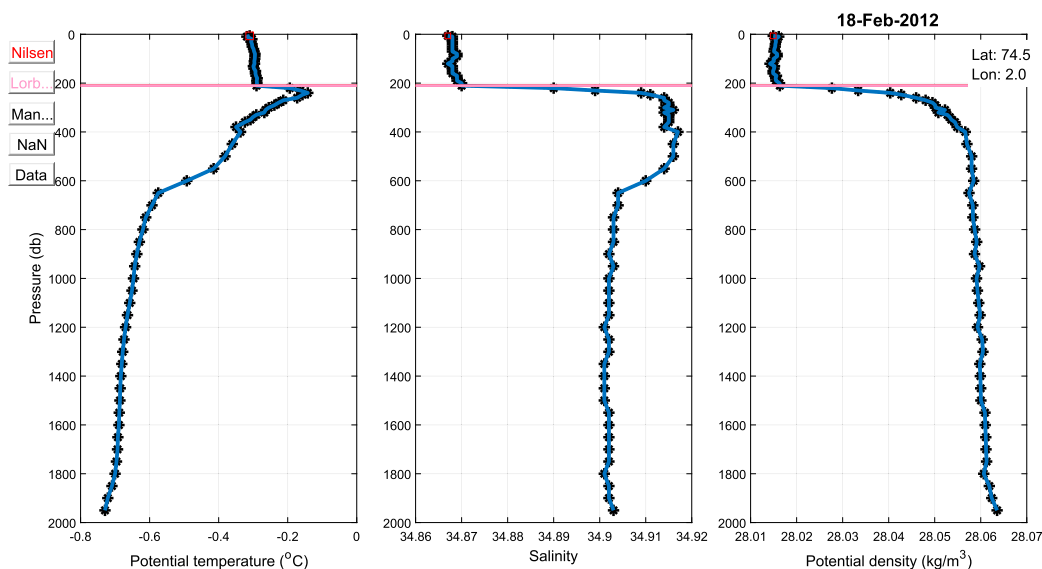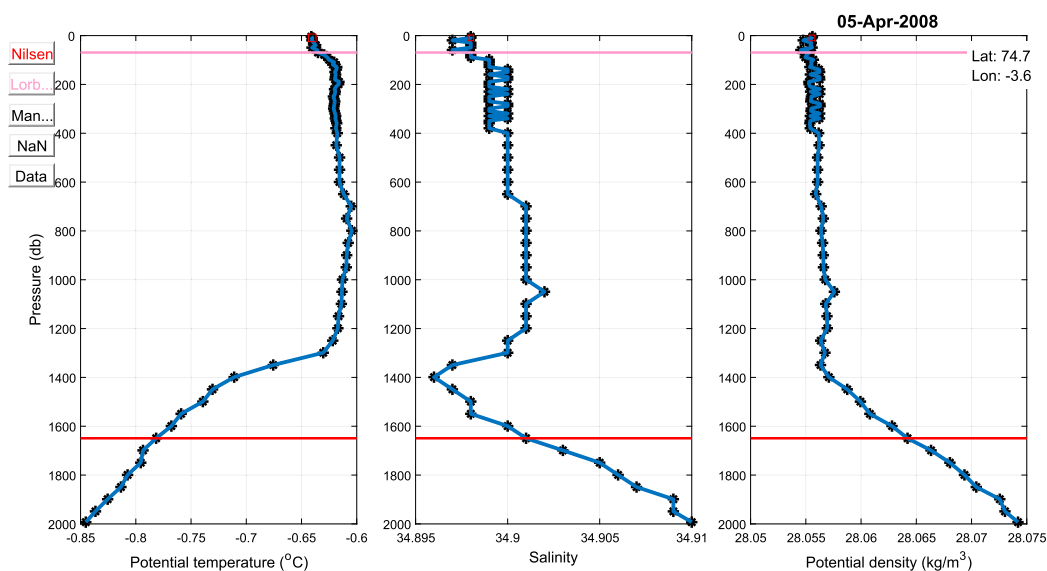
FIG. A1. Examples of two hydrographic profiles from the Greenland Sea gyre, (a) one from February 2012 and (b) one from April 2008. The red and magenta lines indicate the mixed layer depths identified by the density-difference routine and the curvature routine, respectively.

Fram Strait by the EGC was anomalously high during the Great Salinity Anomalies in the late 1980s and late 1990s (Belkin et al. 1998; Belkin 2004), which could be a reason for the low salinities and shallow mixed layers observed in the Greenland Sea during those time periods. The diversion of freshwater into the Greenland Sea is also regulated by the strength of the cyclonic wind stress curl (Malmberg and Jónsson 1997). That is,

shallow convection could also be a result of decreased cyclonic wind forcing that would reduce the cyclonic gyre circulation and, in turn, weaken the polar front between the Greenland Sea and the EGC.

After 1993, a multiyear increase in near-surface salinity lowered the water-column stability in the Greenland Sea. Weaker stratification along with sufficiently strong atmospheric forcing resulted in convection exceeding
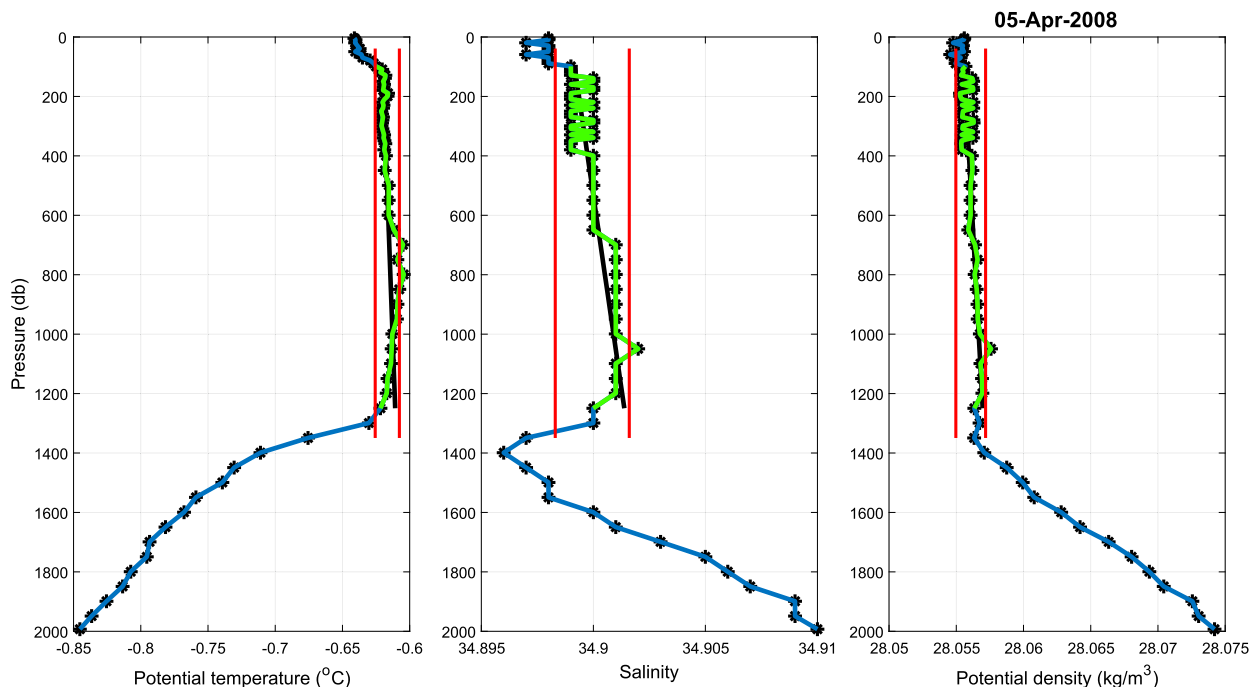
FIG. A2. Illustration of the manual procedure developed by Pickart et al. (2002) for the same hydrographic profile shown in Fig. A1b. The extent of the mixed layer is illustrated in light green, while the vertical red lines indicate plus and minus one standard deviation of the mixed layer properties.

500 m and formation of the new class of GSAIW. Our analysis further suggests that there has been a tendency toward deeper mixed layers during the past 10–15 years. Deeper convection is evident also in the increased volume of GSAIW over the same time period. Hence, there is no indication of predominantly more shallow convection predicted by Moore et al. (2015) if the decreasing trend in atmospheric forcing continues, at least not thus far. The primary reason for this, as suggested by Lauvset et al. (2018), is the weaker stratification within the gyre caused by increased salinities in the upper 1500 m of the water column. Based on a strong cross correlation (0.8, with a 3-yr time lag), they argue that this increase in salinity stems from higher salinities in the Atlantic water that enters the Nordic seas.

The annual mean production of GSAIW from 1994 to 2014 was estimated to 0.6 ± 0.5 Sv and is sufficient to account for roughly 20% of both the NIJ (1.0 ± 0.2 Sv; Harden et al. 2016) and the FBC-overflow (2.2 Sv; Hansen et al. 2016). The contribution may be particularly important for the densest component of the overflow waters (>28.03 kg m^{-3}; Våge et al. 2015; Pickart et al. 2017; Jeansson et al. 2017). We emphasize that the production rate is a minimal estimate as wintertime export of GSAIW was not accounted for. Potential overflow waters formed in areas surrounding the Greenland Sea gyre were also not included in this

estimate. The average summertime export of GSAIW was estimated to 0.9 ± 0.7 Sv. Although tracer release experiments (e.g., Messias et al. 2008) clearly demonstrate export of intermediate water from the Greenland Sea gyre to the surrounding basins in the Nordic seas, further investigations are required in order to determine how and where this export takes place. One possible mechanism that has been suggested is isopycnal mixing with boundary currents such as the EGC (Strass et al. 1993), but whether this mechanism is sufficient to account for the entire export is not clear. If future convection is reduced, either as a result of decreased heat fluxes (e.g., Moore et al. 2015) or because of enhanced near-surface freshwater content (e.g., from increased ice melt), it could impact the overflows both east and west of Iceland and limit the supply of the densest water to the lower limb of the AMOC.

APPENDIX A

Mixed Layer Depths

The vertical extent of the mixed layer was estimated for each hydrographic profile by two independent automated routines. The first routine (used by Nilsen and Falck 2006) was based on a density-difference criterion. The base of the mixed layer was identified as the depth where the increase in potential density reached $\Delta\rho = \rho(T_0 - \Delta T, S_0) - \rho(T_0, S_0)$ where T_0 and S_0 are the measured surface temperature and salinity, respectively, and $\Delta T = 0.2°C$. As Nilsen and Falck (2006), we used a varying $\Delta\rho$ to better account for seasonal changes in the vertical density structure. While Nilsen and Falck (2006) used a temperature difference of $\Delta T = 0.8°C$ in the Norwegian Sea, Våge et al. (2015) found that $\Delta T = 0.2°C$ gave better results for the Iceland Sea due to the weaker stratification there. This applies also to the Greenland Sea; hence, we adopt the same temperature-difference criterion. The second routine [developed by Lorbacher et al. (2006)] identified the base of the mixed layer as the shallowest extremum in the curvature of the temperature profile.

The mixed layer depths estimated by the two automated routines were quality controlled (subjectively) by performing a visual inspection of each hydrographic profile. Examples of two wintertime profiles from the Greenland Sea gyre are shown in Fig. A1. The first example (from February 2012; Fig. A1a) shows a typical profile where both routines successfully estimated the depth of the mixed layer. The profile has a well-defined surface mixed layer down to 210 m that is separated from the deeper part of the water column by a strong density gradient. A typical profile where neither of the two automated routines successfully identified the base of the mixed layer is shown in the second example (from April 2008; Fig. A1b). The weak density gradient between the mixed layer and the deeper part of the water column led to an overestimation by the density-difference routine, while the separation of the mixed layer from the surface caused the curvature routine to underestimate the mixed layer depth. In cases like this,
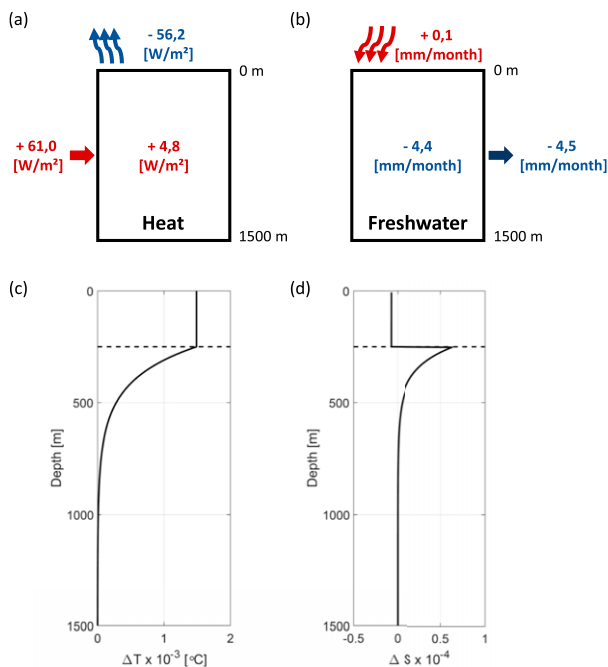

FIG. B1. Annual-mean (a) heat and (b) freshwater budgets for the upper 1500 m of the Greenland Sea gyre. The numbers above each box are the atmospheric fluxes, while the interior changes are shown within each box. The lateral fluxes needed to balance the budgets are indicated by arrows on the sides. The depth distributions of lateral advection of heat and salt, as parameterized in the PWP model, are illustrated by an example of the (c) temperature ΔT and (d) salinity ΔS added for a time step in the model where the mixed layer depth was 500 m. The black dashed lines mark the depth of the mixed layer divided by 2.

we employed a manual procedure developed by Pickart et al. (2002) as illustrated in Fig. A2. The extent of the mixed layer was first estimated visually. Then envelopes of two standard deviations width of the mixed layer temperature, salinity, and density calculated over that depth range were overlaid on the original profiles (vertical red lines in Fig. A2). The vertical limits of the mixed layer were determined as the locations where any one of the profiles last entered the envelope (upper bound) and first exited the envelope (lower bound). The resulting mixed layer extent is marked in light green in the figure.

APPENDIX B

One-Dimensional Mixed Layer Model

a. Vertical mixing

Atmospheric heat, freshwater, and momentum fluxes are imposed at the surface at each time step in the model (Price et al. 1986). Vertical mixing and deepening of the
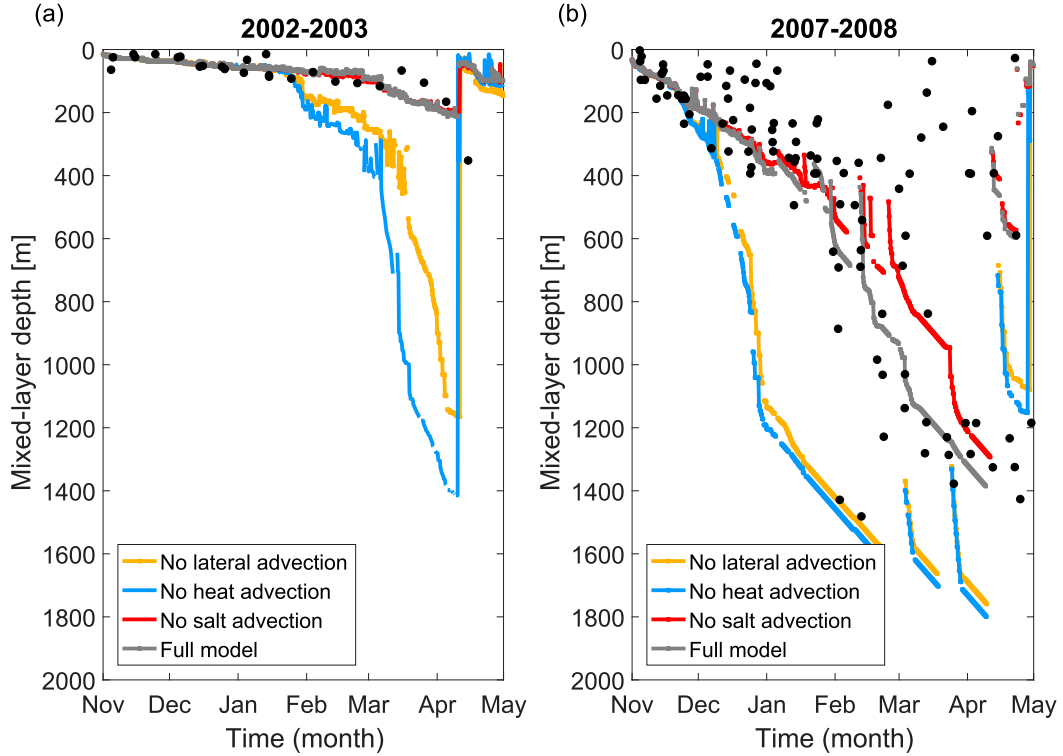
FIG. B2. Seasonal evolution of the mixed layer for (a) a shallow (2002/03) and (b) a deep (2007/08) convective winter. The black dots indicate observed mixed layer depths, while the colored lines show the depth of the mixed layer simulated by the PWP model for four different lateral advection scenarios (see legends).

mixed layer then occur until three different stability criteria are satisfied. The first and most important is the static stability constraint that simulates convection driven by buoyancy loss:

$$\frac{\partial \rho}{\partial z} \geq 0, \tag{B1}$$

where ρ and z are the water density and depth, respectively. When static stability is achieved, the mixed layer is further adjusted by constraining the bulk R_b and gradient R_g Richardson numbers. Mixed layer stability is attained by entrainment when

$$R_b = \frac{g \Delta \rho h}{\rho_0 (\Delta V)^2} \geq 0.6, \tag{B2}$$

where h is the mixed layer depth, V is the velocity (which is driven entirely by wind stress induced momentum), ρ_0 is the reference density, and g is the acceleration due to gravity. In the case of shear flow stability, stirring and deepening take place until

$$R_g = \frac{g \frac{\partial \rho}{\partial z}}{\rho_0 \left(\frac{\partial V}{\partial z}\right)^2} \geq 0.25. \tag{B3}$$

This mixing process is likely to occur across sharp gradients typically found at the base of the mixed layer. Results from sensitivity studies suggest that convection driven by buoyancy loss dominates the mixed layer evolution in the Greenland Sea (not shown).

b. Lateral advection

Annual-mean heat and freshwater budgets for the upper 1500 m of the Greenland Sea gyre from 1986 to 2015 were used to estimate the heat and salt advections (see Figs. B1a,b). To balance the budgets, a lateral heat input to the gyre of 61 W m^{-2}, which is close to the value used by Moore et al. (2015), and a freshwater removal from the gyre of 4.5 mm month^{-1} were required. We assumed constant rates of advection throughout the year. The depth distributions of the heat and salt advections were then determined such that they reflected the temperature and salinity differences across the gyre boundary. For temperature, we used a similar distribution as Moore et al. (2015) as shown in Fig. B1c for a mixed layer depth of 500 m. The distribution of salt is illustrated in Fig. B1d. Salt was removed in the upper half of the mixed layer to account for the input of fresh polar surface water and added below as the surroundings are more saline than the gyre itself. The vertical

distribution of salt advection agrees with the freshwater budgets presented in Latarius and Quadfasel (2016).

We compared the observed and simulated mixed layer depths and properties for each winter. Two winters, one with shallow and one with deep convection, are shown in Fig. B2. Four different simulations are displayed for each winter to illustrate the effect of lateral advection in the model. The exchange of both heat and salt across the gyre boundary must be included in the model in order to realistically simulate the wintertime evolution of the mixed layer. Without advection of heat (blue and yellow curves), the mixed layer depth was greatly over-estimated, while the exchange of salt modified the stratification of the water column resulting in moderately deeper mixed layers (cf. the red and gray curves in Fig. B2b). The simulated mixed layers in our fully parameterized model version (gray) were generally in good agreement with the observations.

c. Sea ice formation

When the simulated sea surface temperature reached the freezing point, we assumed that the net surface heat loss Q_{net} (turbulent and longwave heat fluxes) was used to form sea ice at a rate P following Pickart et al. (2016):

$$P = \frac{Q_{net}}{\rho_{ice} L_n}, \qquad (B4)$$

where the latent heat of fusion L_n and sea ice density ρ_{ice} were set to $300 \, \text{kJ kg}^{-1}$ and $920 \, \text{kg m}^{-3}$, respectively. This is an upper estimate of P since the effect of increasing ice thickness is neglected. That is, the model simulates polynya-like conditions where newly formed sea ice is exported out of the region directly after formation. Wind-driven export of locally formed sea ice was, according to Visbeck et al. (1995), a key process for the evolution of the mixed layer in the Greenland Sea in the late 1980s. The resulting salt flux F_s from brine release was estimated as

$$F_s = \rho_{ice} P (S_w - S_{ice}), \qquad (B5)$$

where S_w is the sea surface salinity and $S_{ice} = 0.31 S_w$ is the salinity of the newly formed sea ice (Cavalieri and Martin 1994). This salt input was added to the upper grid cell at each time step and mixed down in the water column until the stability criteria [Eqs. (B1)–(B3)] were satisfied.

REFERENCES

Aagaard, K., and E. C. Carmack, 1989: The role of sea ice and other fresh water in the Arctic circulation. *J. Geophys. Res.*, **94**, 14 485–14 498, https://doi.org/10.1029/JC094iC10p14485.

——, J. H. Swift, and E. C. Carmack, 1985: Thermohaline circulation in the Arctic Mediterranean Seas. *J. Geophys. Res.*, **90**, 4833–4846, https://doi.org/10.1029/JC090iC03p04833.

Belkin, I. M., 2004: Propagation of the ''Great Salinity Anomaly'' of the 1990s around the northern North Atlantic. *Geophys. Res. Lett.*, **31**, L08306, https://doi.org/10.1029/2003GL019334.

——, S. Levitus, J. Antonov, and S.-A. Malmberg, 1998: ''Great Salinity Anomalies'' in the North Atlantic. *Prog. Oceanogr.*, **41**, 1–68, https://doi.org/10.1016/S0079-6611(98)00015-9.

Carmack, E., and K. Aagaard, 1973: On the deep water of the Greenland Sea. *Deep-Sea Res. Oceanogr. Abstr.*, **20**, 687–715, https://doi.org/10.1016/0011-7471(73)90086-7.

Cavalieri, D. J., and S. Martin, 1994: The contribution of Alaskan, Siberian, and Canadian coastal polynyas to the cold halocline layer of the Arctic Ocean. *J. Geophys. Res.*, **99**, 18 343–18 362, https://doi.org/10.1029/94JC01169.

Chaudhuri, A. H., R. M. Ponte, and A. T. Nguyen, 2014: A comparison of atmospheric reanalysis products for the Arctic Ocean and implications for uncertainties in air–sea fluxes. *J. Climate*, **27**, 5411–5421, https://doi.org/10.1175/JCLI-D-13-00424.1.

Davis, R. E., 1998: Preliminary results from directly measuring middepth circulation in the tropical and South Pacific. *J. Geophys. Res.*, **103**, 24 619–24 639, https://doi.org/10.1029/98JC01913.

Dee, D. P., and Coauthors, 2011: The ERA-Interim reanalysis: Configuration and performance of the data assimilation system. *Quart. J. Roy. Meteor. Soc.*, **137**, 553–597, https://doi.org/10.1002/qj.828.

Eldevik, T., J. E. Ø. Nilsen, D. Iovino, K. A. Olsson, A. B. Sandø, and H. Drange, 2009: Observed sources and variability of Nordic seas overflow. *Nat. Geosci.*, **2**, 406–409, https://doi.org/10.1038/ngeo518.

Fogelqvist, E., J. Blindheim, T. Tanhua, S. Østerhus, E. Buch, and F. Rey, 2003: Greenland–Scotland overflow studied by hydrochemical multivariate analysis. *Deep-Sea Res. I*, **50**, 73–102, https://doi.org/10.1016/S0967-0637(02)00131-0.

Frajka-Williams, E., P. B. Rhines, and C. C. Eriksen, 2014: Horizontal stratification during deep convection in the Labrador Sea. *J. Phys. Oceanogr.*, **44**, 220–228, https://doi.org/10.1175/JPO-D-13-069.1.

Gebbie, G., and P. Huybers, 2010: Total matrix intercomparison: A method for determining the geometry of water-mass pathways. *J. Phys. Oceanogr.*, **40**, 1710–1728, https://doi.org/10.1175/2010JPO4272.1.

Gelderloos, R., F. Straneo, and C. A. Katsman, 2012: Mechanisms behind the temporary shutdown of deep convection in the Labrador Sea: Lessons from the Great Salinity Anomaly years 1968–71. *J. Climate*, **25**, 6743–6755, https://doi.org/10.1175/JCLI-D-11-00549.1.

Hansen, B., K. M. H. Larsen, H. Hátún, and S. Østerhus, 2016: A stable Faroe Bank Channel overflow 1995–2015. *Ocean Sci.*, **12**, 1205–1220, https://doi.org/10.5194/os-12-1205-2016.

Harden, B. E., and Coauthors, 2016: Upstream sources of the Denmark Strait Overflow: Observations from a high-resolution mooring array. *Deep-Sea Res. I*, **112**, 94–112, https://doi.org/10.1016/j.dsr.2016.02.007.

Helland-Hansen, B., and F. Nansen, 1909: The Norwegian Sea: Its physical oceanography based upon the Norwegian researches 1900–1904. Norwegian Fishery and Marine Investigations Rep. Vol. 2, Part 1, No. 2, 390 pp.

Isachsen, P. E., S. R. Sørlie, C. Mauritzen, C. Lydersen, P. Dodd, and K. M. Kovacs, 2014: Upper-ocean hydrography of the Nordic seas during the International Polar Year (2007–2008) as observed by instrumented seals and Argo floats. *Deep-Sea Res. I*, **93**, 41–59, https://doi.org/10.1016/j.dsr.2014.06.012.

Jeansson, E., A. Olsen, and S. Jutterström, 2017: Arctic Intermediate Water in the Nordic seas, 1991–2009. *Deep-Sea Res. I*, **128**, 82–97, https://doi.org/10.1016/j.dsr.2017.08.013.

Jochumsen, K., M. Moritz, N. Nunes, D. Quadfasel, K. M. H. Larsen, B. Hansen, H. Valdimarsson, and S. Jonsson, 2017: Revised transport estimates of the Denmark Strait overflow. *J. Geophys. Res. Oceans*, **122**, 3434–3450, https://doi.org/10.1002/2017JC012803.

Jonsson, S., and H. Valdimarsson, 2004: A new path for the Denmark Strait overflow water from the Iceland Sea to Denmark Strait. *Geophys. Res. Lett.*, **31**, L03305, https://doi.org/10.1029/2003GL019214.

Karstensen, J., P. Schlosser, J. Blindheim, J. Bullister, and D. Wallace, 2003: Formation of intermediate water in the Greenland Sea during the 1990s. *ICES Mar. Sci. Symp.*, **219**, 375–377.

——, ——, D. W. R. Wallace, J. L. Bullister, and J. Blindheim, 2005: Water mass transformation in the Greenland Sea during the 1990s. *J. Geophys. Res.*, **110**, C07022, https://doi.org/10.1029/2004JC002510.

Latarius, K., and D. Quadfasel, 2010: Seasonal to inter-annual variability of temperature and salinity in the Greenland Sea gyre: Heat and freshwater budgets. *Tellus*, **62A**, 497–515, https://doi.org/10.1111/j.1600-0870.2009.00453.x.

——, and ——, 2016: Water mass transformation in the deep basins of the Nordic seas: Analyses of heat and freshwater budgets. *Deep-Sea Res. I*, **114**, 23–42, https://doi.org/10.1016/j.dsr.2016.04.012.

Lauvset, S. K., A. Brakstad, K. Våge, A. Olsen, E. Jeansson, and K. A. Mork, 2018: Continued warming, salinification and oxygenation of the Greenland Sea gyre. *Tellus*, **70A**, 1–9, https://doi.org/10.1080/16000870.2018.1476434.

Lazier, J. R. N., 1980: Oceanographic conditions at ocean weather ship *Bravo*, 1964–1974. *Atmos.–Ocean*, **18**, 227–238, https://doi.org/10.1080/07055900.1980.9649089.

Lorbacher, K., D. Dommenget, P. P. Niiler, and A. Köhl, 2006: Ocean mixed layer depth: A subsurface proxy of ocean-atmosphere variability. *J. Geophys. Res.*, **111**, C07010, https://doi.org/10.1029/2003JC002157.

Malmberg, S.-A., 1983: Hydrographic investigations in the Iceland and Greenland seas in late winter 1971—''Deep water project.'' *Jökull*, **33**, 133–140.

——, and S. Jónsson, 1997: Timing of deep convection in the Greenland and Iceland Seas. *ICES J. Mar. Sci.*, **54**, 300–309, https://doi.org/10.1006/jmsc.1997.0221.

Marnela, M., B. Rudels, I. Goszczko, A. Beszczynska-Möller, and U. Schauer, 2016: Fram Strait and Greenland Sea transports, water masses, and water mass transformations 1999-2010 (and beyond). *J. Geophys. Res. Oceans*, **121**, 2314–2346, https://doi.org/10.1002/2015JC011312.

Marshall, J., and F. Schott, 1999: Open-ocean convection: Observations, theory, and models. *Rev. Geophys.*, **37**, 1–64, https://doi.org/10.1029/98RG02739.

Mastropole, D., R. S. Pickart, H. Valdimarsson, K. Våge, K. Jochumsen, and J. Girton, 2017: On the hydrography of Denmark Strait. *J. Geophys. Res. Oceans*, **122**, 306–321, https://doi.org/10.1002/2016JC012007.

Mauritzen, C., 1996: Production of dense overflow waters feeding the North Atlantic across the Greenland-Scotland Ridge. Part 1: Evidence for a revised circulation scheme. *Deep-Sea Res. I*, **43**, 769–806, https://doi.org/10.1016/0967-0637(96)00037-4.

Meincke, J., S. Jónsson, and J. H. Swift, 1992: Variability of convective conditions in the Greenland Sea. *ICES Mar. Sci. Symp.*, **195**, 32–39.

——, B. Rudels, and H. J. Friedrich, 1997: The Arctic Ocean–Nordic seas thermohaline system. *ICES J. Mar. Sci.*, **54**, 283–299, https://doi.org/10.1006/jmsc.1997.0229.

Messias, M.-J., and Coauthors, 2008: The Greenland Sea tracer experiment 1996–2002: Horizontal mixing and transport of Greenland Sea Intermediate Water. *Prog. Oceanogr.*, **78**, 85–105, https://doi.org/10.1016/j.pocean.2007.06.005.

Moore, G. W. K., K. Våge, R. S. Pickart, and I. A. Renfrew, 2015: Decreasing intensity of open-ocean convection in the Greenland and Iceland seas. *Nat. Climate Change*, **5**, 877–882, https://doi.org/10.1038/nclimate2688.

Nilsen, J. E. Ø., and E. Falck, 2006: Variations of mixed layer properties in the Norwegian Sea for the period 1948–1999. *Prog. Oceanogr.*, **70**, 58–90, https://doi.org/10.1016/j.pocean.2006.03.014.

——, H. Hátún, K. A. Mork, and H. Valdimarsson, 2008: The NISE dataset. Faroese Fisheries Laboratory Tech. Rep. 08-01, 20 pp.

Nøst, O. A., and P. E. Isachsen, 2003: The large-scale time-mean ocean circulation in the Nordic seas and Arctic Ocean estimated from simplified dynamics. *J. Mar. Res.*, **61**, 175–210, https://doi.org/10.1357/002224003322005069.

Østerhus, S., T. Sherwin, D. Quadfasel, and B. Hansen, 2008: The overflow transport east of Iceland. *Arctic–Subarctic Ocean Fluxes*, R. R. Dickson, J. Meincke, and P. Rhines, Eds., Springer, 427–441, https://doi.org/10.1007/978-1-4020-6774-7_19.

Papritz, L., and T. Spengler, 2017: A Lagrangian climatology of wintertime cold air outbreaks in the Irminger and Nordic seas and their role in shaping air–sea heat fluxes. *J. Climate*, **30**, 2717–2737, https://doi.org/10.1175/JCLI-D-16-0605.1.

Pickart, R. S., and W. M. Smethie, 1998: Temporal evolution of the deep western boundary current where it enters the subtropical domain. *Deep-Sea Res. I*, **45**, 1053–1083, https://doi.org/10.1016/S0967-0637(97)00084-8.

——, D. J. Torres, and R. A. Clarke, 2002: Hydrography of the Labrador Sea during active convection. *J. Phys. Oceanogr.*, **32**, 428–457, https://doi.org/10.1175/1520-0485(2002)032<0428:HOTLSD>2.0.CO;2.

——, G. W. K. Moore, C. Mao, F. Bahr, C. Nobre, and T. J. Weingartner, 2016: Circulation of winter water on the Chukchi shelf in early summer. *Deep-Sea Res. II*, **130**, 56–75, https://doi.org/10.1016/j.dsr2.2016.05.001.

——, and Coauthors, 2017: The north Icelandic jet and its relationship to the North Icelandic Irminger Current. *J. Mar. Res.*, **75**, 605–639, https://doi.org/10.1357/002224017822109505.

Price, J. F., R. A. Weller, and R. Pinkel, 1986: Diurnal cycling: Observations and models of the upper-ocean response to diurnal heating, cooling, and wind mixing. *J. Geophys. Res.*, **91**, 8411–8427, https://doi.org/10.1029/JC091iC07p08411.

Quadfasel, D., and J. Meincke, 1987: Note on the thermal structure of the Greenland Sea gyres. *Deep-Sea Res.*, **34A**, 1883–1888, https://doi.org/10.1016/0198-0149(87)90061-6.

Ronski, S., and G. Budéus, 2005: Time series of winter convection in the Greenland Sea. *J. Geophys. Res.*, **110**, C04015, https://doi.org/10.1029/2004JC002318.

Rudels, B., G. Björk, J. Nilsson, P. Winsor, I. Lake, and C. Nohr, 2005: The interaction between waters from the Arctic Ocean and the Nordic seas north of Fram Strait and along the East

Greenland Current: Results from the Arctic Ocean-02 Oden expedition. *J. Mar. Syst.*, **55**, 1–30, https://doi.org/10.1016/j.jmarsys.2004.06.008.

Skagseth, Ø., and K. A. Mork, 2012: Heat content in the Norwegian Sea, 1995–2010. *ICES J. Mar. Sci.*, **69**, 826–832, https://doi.org/10.1093/icesjms/fss026.

Strass, V. H., E. Fahrbach, U. Schauer, and L. Sellmann, 1993: Formation of Denmark Strait overflow water by mixing in the East Greenland Current. *J. Geophys. Res.*, **98**, 6907–6919, https://doi.org/10.1029/92JC02732.

Swift, J. H., and K. Aagaard, 1981: Seasonal transitions and water mass formation in the Iceland and Greenland seas. *Deep-Sea Res.*, **28A**, 1107–1129, https://doi.org/10.1016/0198-0149(81)90050-9.

——, ——, and S.-A. Malmberg, 1980: The contribution of the Denmark Strait overflow to the deep North Atlantic. *Deep-Sea Res.*, **27A**, 29–42, https://doi.org/10.1016/0198-0149(80)90070-9.

Våge, K., R. S. Pickart, G. W. K. Moore, and M. H. Ribergaard, 2008: Winter mixed-layer development in the central Irminger Sea: The effect of strong, intermittent wind events. *J. Phys. Oceanogr.*, **38**, 541–565, https://doi.org/10.1175/2007JPO3678.1.

——, and Coauthors, 2009: Surprising return of deep convection to the subpolar North Atlantic Ocean in winter 2007–2008. *Nat. Geosci.*, **2**, 67–72, https://doi.org/10.1038/ngeo382.

——, R. S. Pickart, M. A. Spall, H. Valdimarsson, S. Jónsson, D. J. Torres, S. Østerhus, and T. Eldevik, 2011: Significant role of the north Icelandic jet in the formation of Denmark Strait overflow water. *Nat. Geosci.*, **4**, 723–727, https://doi.org/10.1038/ngeo1234.

——, ——, ——, G. W. K. Moore, H. Valdimarsson, D. J. Torres, S. Y. Erofeeva, and J. E. Ø. Nilsen, 2013: Revised circulation scheme north of the Denmark Strait. *Deep-Sea Res. I*, **79**, 20–39, https://doi.org/10.1016/j.dsr.2013.05.007.

——, G. W. K. Moore, S. Jónsson, and H. Valdimarsson, 2015: Water mass transformation in the Iceland Sea. *Deep-Sea Res. I*, **101**, 98–109, https://doi.org/10.1016/j.dsr.2015.04.001.

Visbeck, M., J. Fischer, and F. Schott, 1995: Preconditioning the Greenland Sea for deep convection: Ice formation and ice drift. *J. Geophys. Res.*, **100**, 18 489–18 502, https://doi.org/10.1029/95JC01611.

Walsh, J. E., W. L. Chapman, and D. H. Portis, 2009: Arctic cloud fraction and radiative fluxes in atmospheric reanalyses. *J. Climate*, **22**, 2316–2334, https://doi.org/10.1175/2008JCLI2213.1.

Wong, A. P. S., G. C. Johnson, and W. B. Owens, 2003: Delayed-mode calibration of autonomous CTD profiling float salinity data by θ-S climatology. *J. Atmos. Oceanic Technol.*, **20**, 308–318, https://doi.org/10.1175/1520-0426(2003)020<0308:DMCOAC>2.0.CO;2.

Yashayaev, I., and J. W. Loder, 2016: Recurrent replenishment of Labrador Sea Water and associated decadal-scale variability. *J. Geophys. Res. Oceans*, **121**, 8095–8114, https://doi.org/10.1002/2016JC012046.

——, M. Bersch, and H. M. van Aken, 2007: Spreading of the Labrador Sea Water to the Irminger and Iceland basins. *Geophys. Res. Lett.*, **34**, L10602, https://doi.org/10.1029/2006GL028999.